Physical layer simulator of the deep space to ground high photon efficiency optical wireless communications link

Andrew Burton, Zabih Ghassemlooy, Hoa Le Minh
Faculty of Engineering and Environment, Northumbria University, Newcastle upon Tyne, UK
{andrew2.burton; z.ghassemlooy; hoa.le-minh}
@northumbria.ac.uk

Pantelis-Daniel Arapoglou
European Space Agency, European Space Research & Technology Centre (ESTEC), Keplerlaan 1, The Netherlands
pantelis-daniel.arapoglou@esa.int

***Abstract*— This paper focuses on the implementation of the physical layer simulator for the deep space to ground high photon efficiency optical wireless communications link designed by NASA. The link employs the serially concatenated pulse position modulation (SCPPM) transmitted over a cloud free atmospheric and turbulent atmospheric link. The decoder is an iterative process based on the BCJR algorithm to achieve the optimum bit error rate (BER) performance. The results show that for the higher orders of SCPPM a lower signal to noise ratio is required to achieve the same BER as the lower orders. The effects of atmospheric turbulence on the link performance is also demonstrated as well as the combative technique of channel interleaving of the data.**

Keywords—Free-space optics, coding, PPM, space to ground satellite communications.

I. INTRODUCTION

Free-space optical (FSO) communication systems are an emerging technology, and are finding themselves as complementary systems to the traditional radio frequency (RF) and wired fibre links; capable of transmitting up to 1.6 Tbps over a single connection [1]. FSO systems are also being employed to overcome the last mile access network bottleneck as well as the backbone link in cellular systems [2]. Therefore, it is not surprising that FSO is being intensively studied, prototyped and flown as an option to increase the data rate in various space missions. Characteristic examples of recent commercial or experimental space missions that include an optical communications (OC) link is the laser communication terminal (LCT) on board the Alphasat satellite [3], the intersatellite link (ISL) in the European Data Relay System (EDRS) [4] and the Lunar Laser Communication Demonstration (LLCD) link by NASA [5]. Despite the similarities with their microwave counterparts, the physical layer (PL) of OC systems employ specialised FEC coding, modulation and interleaving options. Even for schemes that are in common with radio frequency (RF) communications, signals in the optical domain undergo distinct channel impairments, which give rise to a dedicated PL design. Particularly in space applications, this PL design and, in turn, the offered data rate are shaped by a number of constraints with respect to the technology (e.g., power consumption on board the spacecraft), environment (e.g., thermal control of equipment on board the spacecraft) and regulatory (e.g., eye protection for high power uplink beacons).

The PL of OC for space missions is currently the subject of standardization efforts within the recently established Optical Communications Working Group (OWG) of the Consultative Committee for Space Data Systems (CCSDS) [6]. This group is responsible for developing FSO communications standards to ensure interoperability and cross-support between space agencies. Typical areas these standards cover include modulation, channel coding, interleaving, synchronization, and acquisition of OC signals. The main space mission scenarios on which the CCSDS OWG focuses are: (*i*) deep space for space exploration and science missions; (*ii*) data relay through a geostationary (GEO) satellite acting as a high-speed avenue for downloading high volumes of Earth Observation and other data; and (*iii*) near Earth, e.g., from low earth orbit (LEO) satellites directly transmitting towards ground stations of low complexity. Due to the very different operational requirements for each of these scenarios, a number of different PL configurations are needed for best supporting each, depending among others on (*i*) size and the capabilities of the spacecraft; (*ii*) the received power range (high photon flux vs. low photon flux); (*iii*) the system architecture; and (*iv*) whether the link crosses the atmosphere or not. Using as an example of the modulation formats, deep space OC links typically consider *M*-ary pulsed position modulations (MPPM) [7], data relay systems (such as EDRS) employ a coherent modulation scheme [8], whereas LEO to ground links have adopted on-off keying (OOK) [9]. Furthermore, data relay systems may consist of one or two optical links, which are either ISL or direct to ground links, may require different on board processing. All these options lead to different PL configurations [9-11]. Motivated by this wide range of PL configurations, this paper gives an overview and provides preliminary results of the software (SW) tools developed for simulating the PL in OC systems, in support of the CCSDS OWG as well as of ESA wide activities. The

activity aims at developing SW tools to perform computer simulations of various end-to-end PLs for OC systems, integrated in a single SW platform referred to as end-to-end PL simulator for OC (E2EOPHY).

In this paper the focus is mainly on one of the SW simulator routines that have been developed in the frame of a European Space Agency contract, namely the serially concatenated pulse position modulation (SC-PPM), which is a PL performing within one dB or so from the capacity of the photon counting severely power limited channel [2]. Such characteristics are typically present in deep space missions, where spacecraft's need to communicate back to Earth from link ranges that could potentially be many Astronomical Units. Due to its efficiency, the SC-PPM is considered in a number of deep space optical studies and In Orbit Demonstrations, such as the Deep Space Optical Communications project at the Jet Propulsion Laboratory with the aim to demonstrate laser communication links at transmission ranges of approximately 3 AU [12].

II. SYSTEM DESCRIPTION

The data flow for the deep space high photon efficiency communications link employing SCPPM is shown in Figure 1. The user data consists of a pseudo random bit stream (PRBS) **a** with a constraint length k defined by the code rate r employed. **a** is appended with a 32-bit cyclic redundancy check (CRC) and terminated with two zero binary bits prior to being encoded, see Table I. This is to ensure the input data block length $\hat{k}$ is of $15120r$. The significance of this number is so that **a** can be mapped into $15120/\log_2 M$ symbols, where M is the PPM order, for a range of $M \in \{4, 8, 16, 32, 64, 128, \text{and } 256\}$.

Table I User data lengths.

Code rate r	User data length k	Length of user data with CRC-32 and 2-binary-digit termination $\hat{k}$
1/3	5006	5040
1/2	7526	7560
2/3	10046	10080

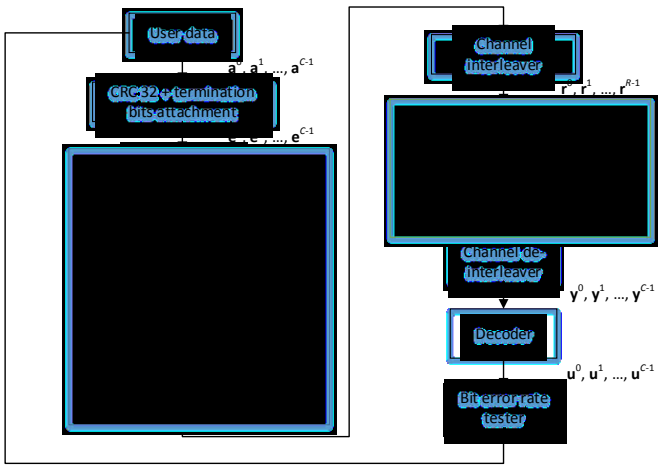

Figure 1 SCPPM encoder/channel/decoder data flow diagram.

The encoder is composed of a convolutional encoder, bit interleaver, accumulator and PPM symbol mapper. The symbols are then interleaved through a convolutional interleaver (different from the bit interleaver) before being transmitted through the free space channel. For a deep space optical wireless link, a photon counting receiver (Rx) is utilised and modelled based on the Poisson distribution statistics [13-15]. Terrestrial atmospheric turbulence effects are also modelled using the log-normal (LN) distribution statistics [16-19] and is defined by means of the scintillation index (SI). The received data **y** is then de-interleaved **Y** at the Rx before being decoded.

The decoding is performed in an iterative process between the inner and outer decoder. Once the maximum number of iterations is reached, or the output decoder estimate **U** satisfies the CRC, the iterations is stopped and the regenerated data bits is produced, which are then compared with **a** in order to determine the bit error rate (BER).

A. CHANNEL MODELS

1) The photon counting Poisson channel

The binary symbols **q** are transmitted over the optical channel $\mathbf{H_c}$ and received as **Y**. The Rx is modelled by a memoryless binary-input Poisson channel $f(_{Y|q})$. It is assumed that the channel has an average K_b background photons per slot, and K_s photons per symbol. Hence, the distributions for the background and signal photons per slot are given by [13, 14]:

$$f_{Y|q}(\mathrm{y}|0) = \frac{K_b^y e^{-K_b}}{y!}, \quad (1)$$

$$f_{Y|q}(\mathrm{y}|1) = \frac{(K_s + K_b)^y e^{-(K_s+K_b)}}{y!}. \quad (2)$$

2) The log-normal atmospheric channel

The transmitted laser beam travelling through the atmosphere will experience the absorption, scattering and intensity fluctuation depending on the atmospheric conditions such as fog, rain, snow, low clouds, and turbulence, smoke and dust particles [20, 21]. However, in FSO communication links losses induced due to the atmosphere are mainly dominated by the fog and turbulence compared to the others [20]. In the absence of fog or other aerosols, turbulence due to temperature inhomogeneity causes corresponding changes in the refractive index of the atmosphere. This creates eddies or cells of varying sizes from ~0.1 cm to ~10 m with different temperatures [16]. These mirrors like cells deviate and fluctuates the optical beam from its original path. Consequently, the optical beam suffers from significant fading and phase distortion [18]. Here, we only consider the weak turbulence, thus have adopted LN distribution, which is most widely used model for the probability density function of the irradiance due to its simplicity, and is given by [20, 21].

$$p(I) = \frac{1}{\sqrt{2\pi\sigma_l^2}}\frac{1}{I}\exp\left\{-\frac{\left(\ln\left(\frac{I}{I_0}\right) - E[l]\right)^2}{2\sigma_l^2}\right\}, \text{for } I > 0. \quad (3)$$

where the log irradiance variance for a plane wave is given by:

$$\sigma_l^2 = 1.23 C_n^2 k^{7/6} L^{11/6}, \quad (4)$$

C_n^2 is the index of refraction structure parameter given as [17]:

$$C_n^2(\hbar) = 0.005(v_w/27)^2(10^{-5}\hbar)^{10}\exp(-\hbar/1000) + 2.7\times10^{-6}\exp(-\hbar/1500) + \hat{\mathrm{A}}\exp(-\hbar/100), \quad (5)$$

where, I and I_0 are the intensity with and without turbulence, respectively, Â is a normal value of C_n^2 (0) at the ground level in $m^{-2/3}$, and $v_w \sim 21$ m/s, and L is the propagation path length. The value of C_n^2 varies with the altitude $\hbar$ of the atmosphere, however, it is almost considered to be constant for a horizontally propagating field. The typical average values of C_n^2 are 10^{-12} $m^{-2/3}$ and 10^{-17} $m^{-2/3}$ for the strong and weak turbulence regimes, respectively [19]. Practically, C_n^2 is a measure of the strength of the fluctuations in the refractive index of the propagation channel. Table II relates the turbulence strength with the different values of SI.

Table II Strength of turbulence based on SI.

Turbulence	SI
Weak	$\sigma_l^2 < 0.3$
Medium	$\sigma_l^2 \approx 1$
Strong	$\sigma_l^2 >> 1$

B. SCPPM encoder and chanel interleaver

1) SCPPM encoder

The encoder consists of the outer and inner codes, and a code interleaver, see Figure 2. The outer code is a short-constraint-length convolutional code, whereas the inner code is composed of an accumulator and a memoryless PPM modulator. The PPM modulator maps each set of $\log_2 M$ codes to a PPM symbol. For a detailed explanation of the SCPPM encoder please refer to [22].

Figure 2 SCPPM encoder and channel

2) Channel iterleaver

The SCPPM codeword sequence ($\mathbf{q}^0$, $\mathbf{q}^1$, …, $\mathbf{q}^{C-1}$) can be regarded as a vector of vectors. However, this sequence can also be re-noted as a single vector, i.e.:

$$\hat{q} = \hat{q}_0, \hat{q}_1, \ldots, \hat{q}_{CS-1}, \quad (6)$$

where $i \in \{0, 1, \ldots, C\text{-}1\}$ and $j \in \{0, 1, \ldots, S\text{-}1\}$, hence $\hat{q}_{iS+j} = q_j^i$. This sequence of PPM symbols is interleaved through a convolutional interleaver. The convolutional interleaver structure is shown in Figure 3. The interleaver has N rows, each containing a shift register of length iB, hence storing iB PPM symbols. Note that, the initial state of the shift registers prior to interleaving does not require initialisation. The initial contents of the interleaver shall be produced at the output during operation, that is $N(N-1)B/2$ symbols. Note, B is the convolutional interleaver register step length. Therefore by the time the last symbol, $\hat{q}_{CS-1}$, has been applied to the interleaver, the interleaver should carry out additional $N(N-1)B/2$ steps to complete the sequence and to appear at the output. Thus, resulting in an output containing $N(N-1)B$ more symbols than the input, which is given as:

$$\hat{\mathbf{r}} = \hat{r}_0, \hat{r}_1, \ldots, \hat{r}_{SC+N(N-1)B-1}. \quad (7)$$

The sequence $\hat{\mathbf{r}}$ is then re-indexed into $R = C + N(N-1)B/S$ blocks, with each block containing S symbols:

$$\mathbf{r} = \mathbf{r}^0, \mathbf{r}^1, \ldots, \mathbf{r}^{R-1}, \quad (8)$$

where for $i \in \{0, 1, \ldots, R\text{-}1\}$, the i^{th} block is denoted as:

$$\mathbf{r}^i = \mathbf{r}_0^i, \mathbf{r}_1^i, \ldots, \mathbf{r}_{S-1}^i, \quad (9)$$

and for $j \in \{0, 1, \ldots, S\text{-}1\}$:

$$r_j^i = \hat{r}_{iS+j}. \quad (10)$$

Each $\boldsymbol{r}^i$ is an interleaved codeword and contains S symbols.

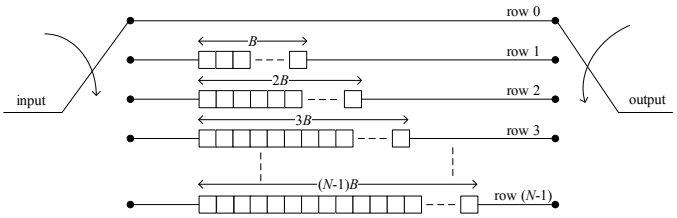

Figure 3 the convolutional channel interleaver (each of the boxes represents a memory element).

C. SCPPM decoder

Figure 4 shows the Rx system block diagram, where the signal is demodulated and decoded to recover the estimated version of the user data **a**. The inner decoder produces an extrinsic output $\Lambda_{OUT}(A'_h)$ for $h = 1, \ldots, n$. This is an estimate of the log likelihood ratio (LLR) of the interleaved code bits A'_h, based on the input signals $\boldsymbol{y}$, a priori LLR estimate $\Lambda_{IN}(A'_h)$ and the structure imposed by the inner code. Following the use of suitable de-interleaving the information is applied to the insert zero module in order to add zeros to the coded bits according to the puncture pattern. Following this, the outer decoder is then able to generate an extrinsic output $\Lambda_{OUT}(X'_h)$ (i.e., an estimate of the LLR of X'_h, the convolutional code output) based on the a priori estimate $\Lambda_{IN}(X'_h)$ and the structure imposed by the outer code. A second output produces a tentative estimate of the decoded bits **U**. If **U** satisfies the CRC-32, then decoding is completed and what are generated are the estimated bits. However, if the CRC-32 condition is not satisfied, then the extrinsic output of the outer decoder is punctured per the puncture pattern and the code rate, which is interleaved and fed back, as the a priori LLR input, to the inner decoder. This entire process continues until the CRC-32 is satisfied or, the maximum number of decoder iterations is

reached. The BER tester compares the estimate **U** with the information block **a**, bit for bit.

1) The inner decoder

The inner decoder has two inputs; the received photon counts *y* and the set of imperfect a priori estimates of the LLR's of the interleaved code bits $A'_1, A'_2, \dots, A'_n$ arriving from the outer decoder. From *y* the log likelihood (LLH) that the i^{th} PPM symbol is *j* can be determined [15, 23]:

$$\ln[P(\mathbf{Y}_i = y_i|\mathbf{q}_i = j)] = y_{i,j}\ln\left[1 + \frac{K_s}{K_b}\right]. \quad (11)$$

The a priori estimates of the LLR's of $A'_1, A'_2, \dots, A'_n$ are defined as [15, 23]:

$$\Lambda_{IN}(A'_h) = \ln\left[\frac{P(A'_h = 1)}{P(A'_h = 0)}\right]. \quad (12)$$

During the first decoding iteration, the outer decoder has not yet had chance to produce an output, therefore the estimate is initialised to:

$$\Lambda_{IN}(A'_h) = 0. \quad (13)$$

The accumulate and PPM (APPM) decoder operates on the BJCR algorithm principle [24], and uses a trellis that is described by two states and *M*/2 parallel branches between the connecting states. The extrinsic output of the inner decoder is composed of the a posteriori LLR of a'_h and the a priori estimates of the LLR's of A'_h, as given by [25]:

$$\Lambda_{OUT}(A'_h) = \Lambda(A'_h) - \Lambda_{IN}(A'_h). \quad (14)$$

2) The outer decoder

The outer decoder runs on the BCJR algorithm as outlined in [27, 29, 30], and is structured along the trellis arrangement of the outer encoder. The input to the outer decoder $\Lambda(X'_h)$ is the de-interleaved inner decoders LLR of the **X**' codebits:

$$\Lambda_{IN}(X'_h) = \ln\left[\frac{P(X'_h = 1)}{P(X'_h = 0)}\right]. \quad (15)$$

The outputs of the decoder are the log a posteriori probabilities (APPs) of the coded symbols $\Lambda_{OUT}(X'_h)$ and the log APPs of the input bits $\Lambda(\mathbf{U})$ defined by [24, 26, 27]:

$$\Lambda(U_i = u) \triangleq \ln\left[\frac{P(U_i = u \mid \mathbf{Y} = \mathbf{y})}{P(U_i = 0 \mid \mathbf{Y} = \mathbf{y})}\right] = \max^*_{e:u(e)=u}(\sigma(e)) - \max^*_{e:u(e)=0}(\sigma(e)), \quad (16)$$

$$\Lambda(C_i = c) \triangleq \ln\left[\frac{P(C_i = c \mid \mathbf{Y} = \mathbf{y})}{P(C_i = 0 \mid \mathbf{Y} = \mathbf{y})}\right] = \max^*_{e:c(e)=u}(\sigma(e)) - \max^*_{e:c(e)=0}(\sigma(e)), \quad (17)$$

$$\Lambda(U) = \ln[P(U_i = u \mid \mathbf{Y} = \mathbf{y})] = \Lambda(U_i = u) - \max^*_{a\in\mathcal{U}}(\Lambda(U_i = a)), \quad (18)$$

$$\Lambda_{OUT}(X'_h) = \ln[P(C_i = c \mid \mathbf{Y} = \mathbf{y})] = \Lambda(C_i = c) - \max^*_{a\in\mathcal{C}}(\Lambda(C_i = a)), \quad (19)$$

where $\mathcal{U}$ is the set of permissible encoder inputs of a trellis stage, and $\mathcal{C}$ is the set of permissible encoder outputs of a trellis stage. The APPs of the coded symbols $\Lambda_{OUT}(X'_h)$ are interleaved and fed back to the inner decoder, whereas the tentative decoded bits are defined by [24]:

$$u_i = \text{sgn}(\Lambda(U_i = 1)). \quad (20)$$

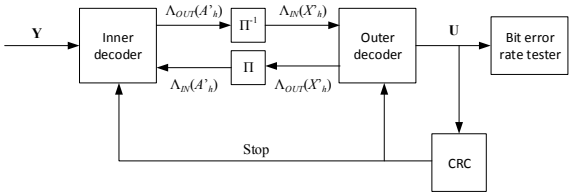

Figure 4 SCPPM decoder and BERT.

III. SIMULATION RESULTS

A. Clear weather simulations

Using the simulation parameters given in Table III, we simulated the system BER performance as a function of the average number of photons per slot K_s/M for the average background photons per slot K_b = 0, 0.01 and 1. A range of *M*-PPM and *r* was selected and for a cloud free conditions. The simulated BER ranges were limited for keeping the simulation time reasonable. As a starting point, in the plots shown in Figures 5 *a-c* there is no fading (i.e. turbulence) included in the channel, only background noise. As can be seen the best BER performance are achieved for higher order of *M* for *r* = 1/3 (*M*= 256), followed by 1/2 (*M* = 128), whereas the worst BER performance is for *r* = 2/3 (*M* = 16). Of course the lowest BER performance is for for K_b = 0 followed by 0.01 and 1. For higher values of K_b = 0 the BER performance decreases for all values of *M* and *r*.

Table III Clear weather simulation parameters.

Parameter	Value
Average number of background photons per slot, K_b	0, 0.01, 1
Average number of photons per slot K_s/M step size	0.1 dB
Code rate, *r*	1/3, 1/2, 2/3
Maximum number of decoder iterations	32
Maximum frame errors	50
Maximum frames to test	700
Number of SCPPM codewords in a sequence, *C*	1
PPM order, *M*	256, 128, 64, 32, 16, 8, 4

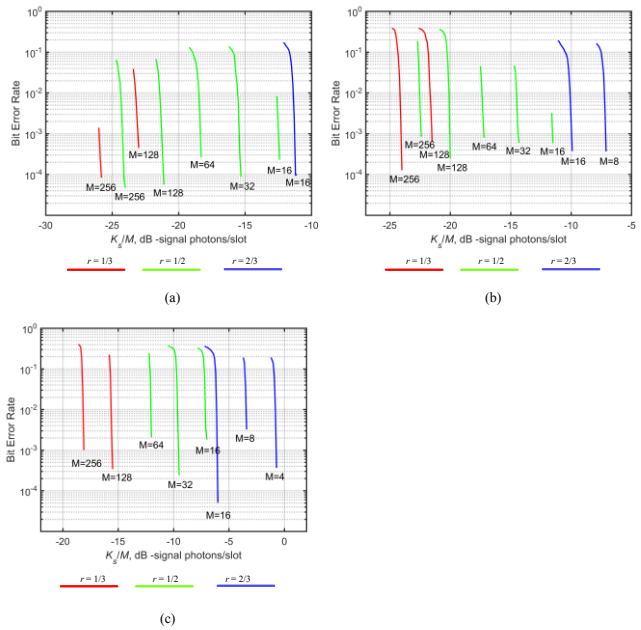

Figure 5 BER results for clear weather with (a) $k_b = 0$, (b) $k_b = 0.01$, and (c) $k_b = 1$.

B. *Atmospheric turbulence effects simulation*

The impact of atmospheric turbulence effects on the BER performance of the proposed communications system for $M = 64$, $r = 1/2$ and $R_b = 2.54$ Mbps with and without the channel interleaver is depicted in Figure 6. The additional simulation parameters are given in Table IV. Note that, turbulence will introduce burst errors, which severely affect the BER performance as shown in Figure 6. However, inclusion of the channel interleaver helps to reduce the burst errors by spreading them over time across many interleaved SCPPM symbols, and following de-interlaving the effect of these errors are greatly reduced, as can be seen from Figure 6. For the case of no SI the BER plots are almost the same with and without channel interleaver. However, for a BER of 10^{-3} and for SI of 0.3 the signal photon/slot penalties are 2 and 4 dB with and without channel interleaver, respectively compared to the case with no SI.

Table IV Additional simulation parameters for atmospheric effects.

Simulation parameter	**Value**
Code rate, r	1/2
Convolutional interleaver register step length, B	120
Convolutional interleaver rows of registers, N	84
PPM order, M	64
Scintillation index, σ_{SI}	0.05, 0.1, 0.2, 0.3
Scintillation fading frequency	400 Hz
User data rate, R_b	2.34 Mbps

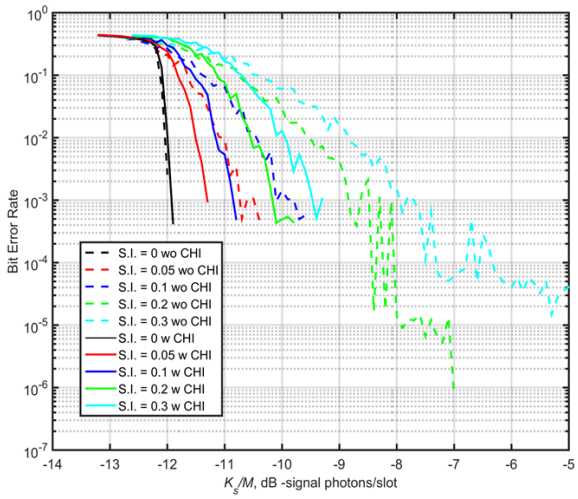

Figure 6 Simulation results for $M = 64$, $r = 1/2$ and $R_b = 2.54$ Mbps through a turbulent channel with and without the channel interleaver.

IV. CONCLUSIONS

The work carried out in this paper was part of software simulation tools that was developed at Northumbria University for the European Space Agency. The theme of this paper was limited to independently verifying SCPPM high efficiency deep space communications PL performance as part of the ongoing standardization work in CCSDS. We showed that the best and worth BER performance were achieved for higher order of $M = 2656$ ($r = 1/3$) and $M = 16$ ($r = 2/3$), respectively. We also showed that the channel interleaver reduced the turbulence induced burst errors by spreading them over time across many interleaved SCPPM symbols. Interesting future extensions of this work involve including detailed receiver synchronization algorithms (e.g., frame, slot and symbol timing synchronization) to understand the performance degradation under practical receiver conditions. Other areas of interest is to add to the simulator specialized detector modelling, such as the superconducting nanowire single photon detector.

V. ACKNOWLEDGEMENT

The authors would like to acknowledge the ESA and NASA for providing all the data and information required to support this work. This work is supported by the ESA under the end-to-End Physical Layer Simulator for Optical Communications (ESA REF/NC/IPL-PTE/FE/mo/342.205).

VI. REFERENCES

[1] N. A. M. Nor, E. Fabiyi, M. M. Abadi, X. Tang, Z. Ghassemlooy, and A. Burton, "Investigation of moderate-to-strong turbulence effects on free space optics - A laboratory demonstration," in *2015 13th International Conference on Telecommunications (ConTEL)*, pp. 1-5, 2015.

[2] M. M. Abadi, Z. Ghassemlooy, D. Smith, and W. P. Ng, "A report on H-FSO/RF antenna measurement for outdoor applications," in

2013 2nd International Workshop on Optical Wireless Communications (IWOW), pp. 118-122, 2013.

[3] T. Spacecom and D. ESA ESOC, "Alphasat TDP1 Three years optical GEO data relay operations," 2016.

[4] F. Heine, G. Mühlnikel, H. Zech, S. Philipp-May, and R. Meyer, "The European Data Relay System, high speed laser based data links," in *Advanced satellite multimedia systems conference and the 13th signal processing for space communications workshop (ASMS/SPSC), 2014 7th*, pp. 284-286, 2014.

[5] D. M. Boroson, J. J. Scozzafava, D. V. Murphy, B. S. Robinson, and M. I. T. Lincoln, "The Lunar Laser Communications Demonstration (LLCD)," in *2009 Third IEEE International Conference on Space Mission Challenges for Information Technology*, pp. 23-28, 2009.

[6] (February 2017). *CCDS technical Organization*. Available: http://cwe.ccsds.org/default.aspx

[7] H. Hemmati, A. Biswas, and I. B. Djordjevic, "Deep-Space Optical Communications: Future Perspectives and Applications," *Proceedings of the IEEE,* vol. 99, pp. 2020-2039, 2011.

[8] F. Heine, G. Mühlnikel, H. Zech, S. Philipp-May, and R. Meyer, "The European Data Relay System, high speed laser based data links," in *2014 7th Advanced Satellite Multimedia Systems Conference and the 13th Signal Processing for Space Communications Workshop (ASMS/SPSC)*, , pp. 284-286 2014.

[9] H. Henniger, A. Ludwig, and J. Horwath, "Performance bounds of DPSK and OOK for low elevation optical LEO downlinks," *Radioengineering,* vol. 1, pp. 589-595, 2010.

[10] S. Dimitrov, B. Matuz, G. Liva, R. Barrios, R. Mata-Calvo, and D. Giggenbach, "Digital modulation and coding for satellite optical feeder links," in *2014 7th Advanced Satellite Multimedia Systems Conference and the 13th Signal Processing for Space Communications Workshop (ASMS/SPSC)*, pp. 150-157, 2014.

[11] B. Friedrichs and P. Wertz, "Error-control coding and packet processing for broadband relay satellite networks with optical and microwave links," in *2012 6th Advanced Satellite Multimedia Systems Conference (ASMS) and 12th Signal Processing for Space Communications Workshop (SPSC)*, pp. 101-110, 2012.

[12] M. Srinivasan, R. Rogalin, N. Lay, M. Shaw, and A. Tkacenko, "Downlink receiver algorithms for deep space optical communications," in *Proc. of SPIE Vol*, pp. 100960A-1, 2017.

[13] Y. Tan, J. z. Guo, Y. Ai, W. Liu, and Y. J. Fei, "A Coded Modulation Scheme for Deep-Space Optical Communications," *IEEE Photonics Technology Letters,* vol. 20, pp. 372-374, 2008.

[14] B. Moision and J. Hamkins, "Deep-space optical communications downlink budget: modulation and coding," *IPN Progress Report,* vol. 42, pp. 1-28, 2003.

[15] M. K. Cheng, B. E. Moision, J. Hamkins, and M. A. Nakashima, "SAT05-4: Implementation of a Coded Modulation for Deep Space Optical Communications," in *IEEE Globecom 2006*, pp. 1-5, 2006.

[16] V. R. Gudimetla, R. B. Holmes, C. Smith, and G. Needham, "Analytical expressions for the log-amplitude correlation function of a plane wave through anisotropic atmospheric refractive turbulence," *JOSA A,* vol. 29, pp. 832-841, 2012.

[17] J. Vitásek, J. Látal, S. Hejduk, J. Bocheza, P. Koudelka, J. Skapa*, et al.*, "Atmospheric turbulences in Free Space Optics channel," in *2011 34th International Conference on Telecommunications and Signal Processing (TSP)*, pp. 104-107, 2011.

[18] S. Takashi, T. Morio, and T. Hideki, "Fading Simulator for Satellite-to-Ground Optical Communication," *Journal of the National Institute of Information and Communications Technology,* vol. 59, pp. 95-102, 2012.

[19] J. Libich and S. Zvanovec, "Influences of turbulences in near vicinity of buildings on free-space optical links," *IET Microwaves, Antennas & Propagation,* vol. 5, pp. 1039-1044, 2011.

[20] M. Uysal and H. Nouri, "Optical wireless communications - An emerging technology," in *2014 16th International Conference on Transparent Optical Networks (ICTON)*, pp. 1-7, 2014.

[21] Z. Ghassemlooy, W. Popoola, and S. Rajbhandari, *Optical wireless communications: system and channel modelling with Matlab®*: CRC press, 2012.

[22] A. Burton, Z. Ghassemlooy, and P. D. Arapoglou, "Physical layer solutions for optical communications in space," in *2016 10th International Symposium on Communication Systems, Networks and Digital Signal Processing (CSNDSP)*, pp. 1-6 , 2016.

[23] B. Moision and J. Hamkins, "Coded modulation for the deep-space optical channel: serially concatenated pulse-position modulation," *IPN Progress Report,* vol. 42, pp. 1-26, 2005.

[24] J. R. Barry, E. A. Lee, and D. G. Messerschmitt, *Digital communication*: Springer Science & Business Media, 2012.

[25] M. F. Barsoum, B. Moision, M. P. Fitz, D. Divsalar, and J. Hamkins, "EXIT Function Aided Design of Iteratively Decodable Codes for the Poisson PPM Channel," *IEEE Transactions on Communications,* vol. 58, pp. 3573-3582, 2010.

[26] K. D. Rao, *Channel coding techniques for wireless communications*: Springer, 2015.

[27] W. W. Peterson and E. J. Weldon, *Error-correcting codes*: MIT press, 1972.